Dynamically balanced absolute sea level of the global ocean derived from near-surface velocity observations

Pearn P. Niiler,[1] Nikolai A. Maximenko,[2,3] and James C. McWilliams[4]

Received 12 September 2003; accepted 23 October 2003; published 25 November 2003.

[1] The 1992–2002 time-mean absolute sea level distribution of the global ocean is computed for the first time from observations of near-surface velocity. For this computation, we use the near-surface horizontal momentum balance. The velocity observed by drifters is used to compute the Coriolis force and the force due to acceleration of water parcels. The anomaly of horizontal pressure gradient is derived from satellite altimetry and corrects the temporal bias in drifter data distribution. NCEP reanalysis winds are used to compute the force due to Ekman currents. The mean sea level gradient force, which closes the momentum balance, is integrated for mean sea level. We find that our computation agrees, within uncertainties, with the sea level computed from the geostrophic, hydrostatic momentum balance using historical mean density, except in the Antarctic Circumpolar Current. A consistent horizontally and vertically dynamically balanced, near-surface, global pressure field has now been derived from observations. *INDEX TERMS:* 4532 Oceanography: Physical: General circulation; 4512 Oceanography: Physical: Currents; 4599 Oceanography: Physical: General or miscellaneous; 4594 Oceanography: Physical: Instruments and techniques. **Citation:** Niiler, P. P., N. A. Maximenko, and J. C. McWilliams, Dynamically balanced absolute sea level of the global ocean derived from near-surface velocity observations, *Geophys. Res. Lett.*, *30*(22), 2164, doi:10.1029/2003GL018628, 2003.

1. Background

[2] Observations of ocean circulation below the surface are sparse, so oceanographers use the "dynamical method" of computing the large spatial scale circulation [*Defant*, 1961]. This method uses the measurements of the oceanic density, e.g., as derived from temperature and salinity described in the World Ocean Atlas 2001 [*Conkright et al.*, 2002] (WOA01), and assumes a hydrostatic momentum balance in the vertical direction and a geostrophic momentum balance in the horizontal direction. From these balances it follows that the horizontal gradient of the density field is proportional to the vertical gradient of the geostrophic circulation [*Pedlosky*, 1987]. Provided a reference geostrophic velocity is known at some depth, the absolute geostrophic circulation at other depths can be computed [*Reid*, 1994]. Here we show how near-surface observations of velocity can be used to obtain the absolute sea level for the global ocean, which can then be used as a reference for computing the dynamic height, or absolute pressure, with depth.

[3] Recently, a global, 10-year data set of near-surface velocity has been obtained with drifting buoys [*Niiler*, 2001]. From these data a geostrophic velocity field near the surface is derived, after subtracting the wind-driven, or Ekman, currents [*Ralph and Niiler*, 1999]. Our results are presented in terms of the absolute sea level distribution that this near-surface geostrophic circulation maintains. The sea level distribution derived from the velocity field is compared with those derived by the aforementioned use of the density field. Satellite-derived gravity and altimeter data can also be used for computing the large-scale absolute sea level, and a comparison with such data can be made soon [*Tapley*, 1997].

2. Methods

[4] The velocities are derived from ARGOS satellite observations of the displacements of drifters with drogues centered at 15m-depth for the period October 1992 to October 2002, for which contemporaneous altimeter observations processed by *Aviso* [1996] are available. *Niiler* [2001] describes the construction and water-following capabilities of the drifters, their deployment procedures, and the data processing. We average the drifter positions and velocities over two inertial periods along the drifter track and then interpolate to 6-hourly values. The 6-hourly velocity observations within 1° latitude × 1° longitude boxes are ensemble-averaged to form a mean velocity.

[5] The wind-driven, or Ekman, velocity is computed at 6-hourly intervals along the drifter track from the empirically fit, complex-notation formula [*Ralph and Niiler*, 1999],

$$\mathbf{V}_E = A \cdot |f|^{-1/2} \cdot \mathbf{W} \cdot \exp(\mathbf{i} \cdot \theta), \quad (1)$$

where $\mathbf{V}_E = U_E + \mathbf{i} \cdot V_E$ is the Ekman current at 15 m depth, $A = 7 \cdot 10^{-7}\ s^{-1/2}$, f is the Coriolis parameter and $\mathbf{W} = W_x + \mathbf{i} \cdot W_y$ is the NCEP reanalysis 10 m height wind interpolated to each drifter track and $\exp(\mathbf{i} \cdot \theta)$ ($\theta = \pm 54°$) represents the rotation of the Ekman current to the right [left] of the wind vector in the northern [southern] hemisphere. The ensemble average of the Ekman velocity is computed the same way as the drifter velocity. The Ekman velocity $\mathbf{V}_E$ is subtracted from the drifter velocity, $\mathbf{V}_D$, and a drifter-sample time-mean (denoted by $\{.\}$), geostrophic velocity, $\{\mathbf{V}_G\}$, is

[1] Scripps Institution of Oceanography, University of California and San Diego, USA.
[2] International Pacific Research Center, SOEST, University of Hawaii, USA.
[3] Also at P. P. Shirshov Institute of Oceanography, Russian Academy of Sciences, Russia.
[4] University of California, Los Angeles, USA.

0094-8276/03/2003GL018628$05.00

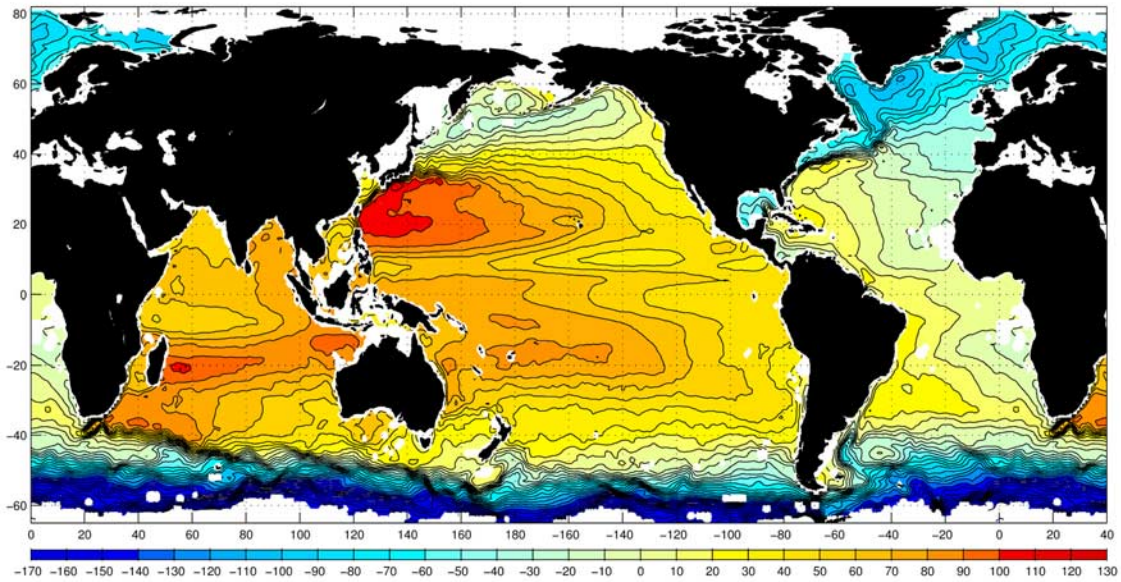

Figure 1. 1992–2002 mean absolute sea level η_0 obtained as described in this paper. Contour interval is 10 cm. Sea level is computed from the values of $\nabla\langle\eta\rangle$ estimated according to (2) on 1° spatial grid with the condition of zero global mean.

derived. An adjustment is then made for the time sampling bias of the drifters with altimeter-derived, geostrophic velocity observations [*Niiler et al.*, 2003], as now described.

[6] The horizontal momentum equation for the 10-year time-averaged sea level, $\langle\eta\rangle$, is [*Pedlosky*, 1987]

$$g\nabla\langle\eta\rangle = -\mathbf{f}\times\left\{\mathbf{V}_G - \mathbf{V}'_S\right\} - \{d\mathbf{V}/dt\}, \qquad (2)$$

where $\{d\mathbf{V}/dt\}$ is the drifter ensemble average of the acceleration following the drifter motion and $\{\mathbf{V}'_S\}$ is the altimeter-derived, time-dependent, anomaly of geostrophic velocity averaged over drifter observations. Over the 10-year, regularly sampled interval, $\langle\mathbf{V}'_S\rangle = 0$. Since irregularly distributed drifter observations can be biased in time over the 10-year period, the quantity $\{\mathbf{V}_G - \mathbf{V}'_S\}$ is the unbiased geostrophic velocity. Similar unbiasing was done by *Uchida and Imawaki* [2003] who assumed that surface currents are in geostrophic balance. Unlike their equation (2), all terms of our (2) remain finite on equator and allow global integration of mean sea level.

[7] A solution, η_0, for $\langle\eta\rangle$ is found by fitting a surface through the finite-difference form of (2) in the global least-square sense, with the constraint that the global average of η_0 is zero (Figure 1). To estimate how well η_0 corresponds to $\langle\eta\rangle$, a potential, φ, is evaluated from the equation,

$$\nabla\varphi = \mathbf{k}\times\nabla(\eta_0 - \langle\eta\rangle) \qquad (3)$$

with the same technique as used to construct a solution for η_0. Substituting from (2) and taking the divergence of (3) yields

$$\nabla^2\varphi = \nabla\cdot(f\cdot\{\mathbf{V}_G - \mathbf{V}'_S\}) + \mathbf{k}\cdot(\nabla\times\{d\mathbf{V}/dt\}). \qquad (4)$$

In the absence of errors, the right side of (4), or the curl of the right side of (2), must vanish, but in practice this does not occur. The potential φ measures the error introduced in to the solution η_0 due to the fact that the right side of (2) is not curl-free. Solving for φ in a global least-square to the derivatives defined in (3) is formally equivalent to solving (4) with a normal boundary derivative specified by the normal component of the right side of (3) [*Salmon*, 1998]. The global root-mean-square value of φ is 6.5 cm, and the values for Pacific, Atlantic and Indian oceans north of 40°S are 7.8, 3.7 and 4.1 cm, respectively.

3. Discussion

[8] The global sea level derived by use of near-surface velocity observations and the horizontal momentum balance (Figure 1) confirms the large-scale spatial patterns north of 40°S that have been derived by the "dynamical method". For comparisons we use *Reid*'s [1994, 1997, 2003] "adjusted steric height at 0 db" and the 3000 m relative steric height we computed from WOA01 (Table 1). The difference of mean sea level across the subtropical basins ([c] in Table 1) and between the subtropical highs and sub-polar lows ([d] in Table 1) with the three different methodologies is 13 cm. The exception is in the subtropical North Atlantic, which in our map is due to a displacement to the east of the high sea level because of a strong, narrow, geostrophic Azores Current not present in Reid's or WOA01's. The disparity between Reid's computation and the other two in the Indian Ocean appears to be caused by the dearth of data directly east of Madagascar. The root-mean-square dynamic heights at 3000 m relative to our absolute surface value, in the basins north of 40°S, are 5.8, 7.2 and 7.2 cm for Pacific, Atlantic and Indian oceans, respectively.

[9] The largest differences between our sea level and the WOA01 3000 m-referenced sea level occur in the Circumpolar Current System, south of 40°S (row 5 of Table 1). The surface geostrophic velocity derived from the drifter data is also stronger than what is obtained from WOA01 referenced to the float observations at 900 m depth [*Gille*, 2003]. We estimate that the 3-basin average surface dynamic height

Table 1. Sea Level Differences Across Basins (cm)

#[a]	Ocean Basin	Coordinates	Reid[b]	WOA01	This study
1	N. Pacific[c]	30°N, 135°E–120°W	85	80	86
2	N. Pacific[d]	30°N, 140°E–50°N, 165°E	140	132	144
3	S. Pacific[c]	18°S, 170°E–80°W	57	64	47
4	N. Atlantic[c]	30°N, 75°W–15°W	55	50	35
5	N. Atlantic[d]	30°N, 75°W–60°N, 45°W	133	137	121
6	S. Atlantic[c]	30°S, 30°W–14°E	40	37	44
7	Indian[c]	20°S, 55°E–35°S, 115°E	40	61	59
8	Southern[e]	60°S–40°S, 160°W–80°W	-	110	210(168)[f]
9	Southern[e]	60°S–40°S, 40°W–20°E	-	140	222(200)[f]
10	Southern[e]	60°S–40°S, 23°E–63°E	-	160	271(225)[f]

[a]Numbers in Figure 3.
[b]From *Reid* [1994, 1997, 2003].
[c]Across subtropical gyres.
[d]Between subtropical high and subpolar low.
[e]Zonal average of meridional difference.
[f]For full dataset and for wind lower than 8 m/s.

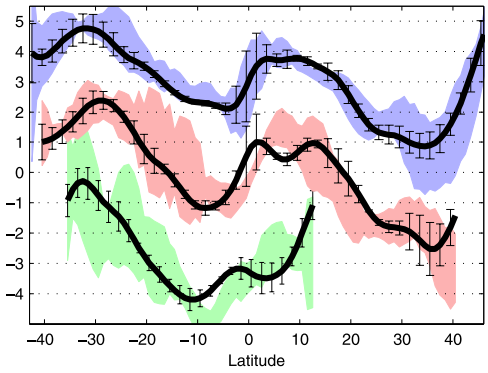

Figure 2. Meridional distributions of zonal mean $\nabla\cdot(f\cdot\{\mathbf{V}_D - \mathbf{V}'_S\}) + \mathbf{k}\cdot(\nabla\times\{d\mathbf{V}/dt\})$ (color strips indicate values deviating from the mean by less than the standard error) and $\nabla\cdot(f\cdot\{\mathbf{V}_E\})$ (mean profiles and standard error bars are in black) averaged over the Pacific (blue), Atlantic (red), and Indian (green) oceans in 5° latitude bands that exclude regions within 200 km of the basin boundaries. Units are 10^{-15} s^{-2}. Pacific/Indian ocean data graphs are shifted up/down by three units.

difference from 60°S to 40°S referenced to the floats is 155 cm, which implies an average zonal surface geostrophic current of 6.3 cm/sec. The sea level difference derived from drifter observations is 234 cm, or average zonal current of 9.6 cm/sec. The winds in this southern ocean are persistently larger than 8 m/sec, with concomitant large surface waves; this is above the range for which drifter slip calibrations were obtained [*Niiler*, 2001]. We re-computed the absolute sea level for winds observed by drifters less than 8 m/s, where average sea level difference is reduced to 198 cm. This reduction indicates that the large winds and ocean waves produce slip of drogues or displacements by the Stokes drift that need to be directly measured in the Circumpolar Current to resolve the discrepancy among the sea level estimates.

[10] The sea level computed by the use of the horizontal momentum equation is sensitive to the choice of the model of Ekman velocity $\mathbf{V}_E$, which accounts for about 50% of the east to west sea level differences across the basins. Our model was derived [*Ralph and Niiler*, 1999] by use of density data [*Levitus*, 1982] and a limited drifter data set in the Pacific within 30° of the equator. An independent test of the efficacy of the Ekman velocity model is shown in Figure 2, which displays $\nabla\cdot(f\cdot\{\mathbf{V}_D - \mathbf{V}'_S\}) + \mathbf{k}\cdot(\nabla\times\{d\mathbf{V}_D/dt\})$ and $\nabla\cdot(f\cdot\{\mathbf{V}_E\})$ averaged in 5° latitude bands that exclude regions 200 km from the basin boundaries. The Ekman velocity model in (1) achieves the basin-scale vorticity balance within uncertainties. Our model of the Ekman current is linear in wind speed and does not depend upon the upper-ocean stratification. Observations and modeling of upper ocean currents call to question the validity of such a simple approach on a global basis [*Large et al.*, 1994], especially in high wind and wave conditions.

[11] While the nonlinear effects of the oceanic mesoscale have been included in the term $\{d\mathbf{V}/dt\}$, the momentum convergence due to surface gravity waves and their effect on the momentum balance has not. Wave-momentum convergences can result in wave forces that produce time-mean sea level signals at sub-polar latitudes in excess of 10 cm [*McWilliams and Restrepo*, 1999]. The Stokes drift within

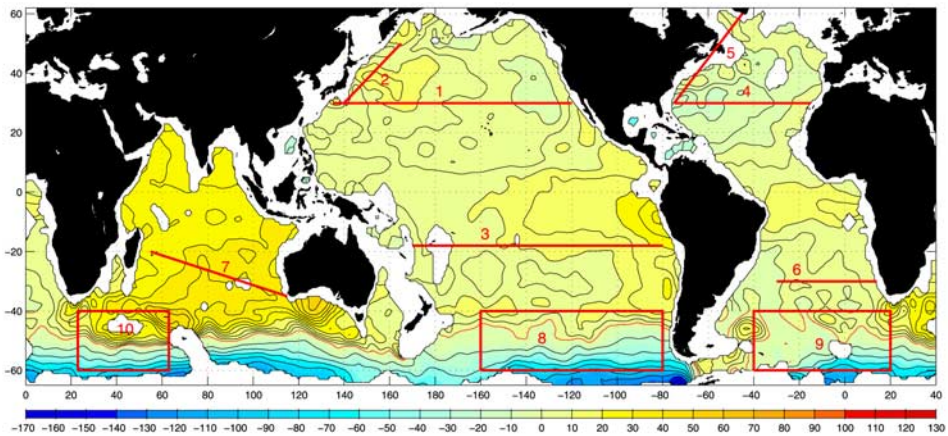

Figure 3. Distribution of pressure anomaly (in dyn.cm) at 3000 m estimated from the mean sea level shown in Figure 1 and dynamic topography relative to 3000 m level calculated from WOA01. Contour interval is 20 cm for negative values (south of red contour) south of 40°S and 5 cm elsewhere. Color scale is same as in Figure 1. Global mean value is subtracted. Numbers indicate segments and boxes listed in Table 1.

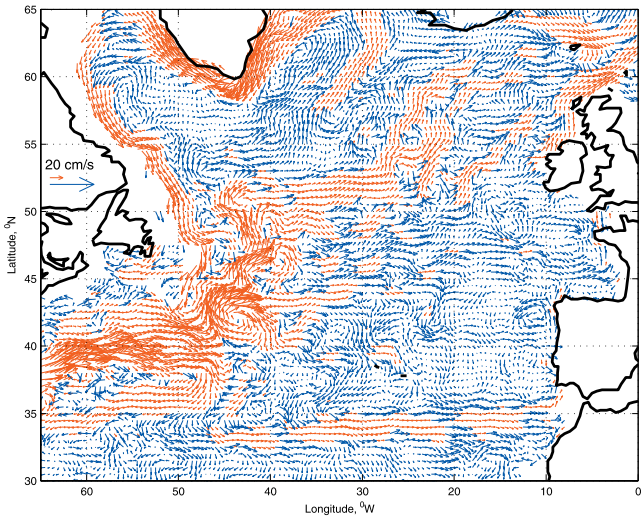

Figure 4. The unbiased mean geostrophic velocity, $\{\mathbf{V}_G - \mathbf{V}'_S\}$, at 15 m depth in the North Atlantic with a 1/2° spatial resolution and averaged from October 1992 to October 2002. Vectors larger than 5 cm/s are shown in red. 20 cm/s scales are displayed in the upper left corner.

several meters of the surface for 10 m/s winds is estimated to be in excess of 30 cm/s in the direction of the wind [*McWilliams and Restrepo*, 1999] and could well be the cause of the increased slip of drifter drogues down wind. Neither of these effects was considered here, but they must be in a more complete analysis.

[12] As seen in Figure 3, the 3000 m-level absolute dynamic heights computed from the difference of η_0 in Figure 1 and the WOA01 3000 m relative steric level depict peak-to-peak variations of 15 cm north of 40°S. These variations are comparable to the uncertainty of the determination of sea level from (2), and large-scale geostrophic circulations of less than 0.5 cm/s can maintain these dynamic height differences at depth over the spatial scales exhibited. While large-scale, time-mean currents of less than 1 cm/s have been observed with floats [*Davis*, 1998], they are beyond the accuracy of drifter observations, the model for the Ekman force, or the sampling uncertainty for the mean velocity in the presence of intense, upper-ocean, time-variable flows.

[13] Strong abyssal velocities suggested by Figure 3 in the Antarctic Circumpolar Current outline the same pattern of deep pressure field as the one derived from the ALACE floats [*Gille*, 2003], but they significantly exceed float velocities. The explanation of this difference probably lies in the correction required to (1), which was derived [*Ralph and Niiler*, 1999] for mid-latitudes.

[14] Besides providing an absolute sea level within 10–15% of the large-scale changes across the major ocean basins, near-surface velocity observations also provide circulation maps of high spatial resolution that cannot be obtained by any other method today. An example is in the North Atlantic, geostrophic velocity (Figure 4) that shows the Azores Current arising with a clear connection to the Gulf Stream recirculation at 33°N, 46°W. The Azores Current then flows eastward as a 100 km wide current. When it reaches the southern part of the Gulf of Cadiz 3500 km to the east, its axis has moved northward by about 100 km. Figure 4 also clearly depicts a strong, narrow current system that follows the 1000 m depth contour around the Irminger and the Labrador basins.

[15] **Acknowledgments.** This research was sponsored by NOAA NA17RJ1231 and NASA NAG5-8351 at SIO and by NSF OCE 01-37077 at UCLA and IPRC. IPRC is partly sponsored by Frontier Research System for Global Change. IPRC/SOEST contribution 246/6287.

References

Archiving, Validation, and Interpretation of Satellite Oceanographic Data (AVISO), in *Aviso Handbook for Merged TOPEX/Poseidon products*, 3rd ed., Toulouse, France, 1996.

Conkright, M. E., R. A. Locarnini, H. E. Garcia, T. D. O'Brian, T. P. Boyer, C. Stephens, and J. I. Antonov, World Ocean Atlas 2001: Objective analysis, data statistics, and figures, *CD-ROM Documentation*, National Oceanographic Data Center, Silver Spring, MD, 17 pp., 2002.

Davis, R. E., Preliminary results from directly measuring middepth circulation in the tropical and South Pacific, *J. Geophys. Res.*, *103*(C11), 24,619–24,639, 1998.

Defant, A., *Physical oceanography*, 729 pp., Oxford, Pergamon Press, 1961.

Gille, S. T., Float observations of the Southern Ocean. Part I: Estimating mean fields, bottom velocities, and topographic steering, *J. Phys. Oceanogr.*, *33*, 1167–1181, 2003.

Large, W. G., J. C. McWilliams, and S. C. Doney, Oceanic vertical mixing: A review and a model with a nonlocal boundary layer parameterization, *Rev. Geophys.*, *32*(4), 363–403, 1994.

Levitus, S., Climatological Atlas of the World Ocean, NOAA Prof. Paper No. 13, U.S. Government Printing Office, 173 pp., 1982.

McWilliams, J. C., and J. M. Restrepo, The wave-driven ocean circulation, *J. Phys. Oceanog.*, *29*, 2523–2540, 1999.

Niiler, P., The World Ocean Surface Circulation, in *Ocean Circulation and Climate-Observing and Modeling the Global Ocean*, edited by J. Church, G. Siedler, and J. Gould, pp. 193–204, Academic, London, 2001.

Niiler, P. P., N. A. Maximenko, G. G. Panteleev, T. Yamagata, and D. B. Olson, Near-surface Dynamical Structure of the Kuroshio Extension, *J. Geophys. Res.*, *108*(C6), 3193, doi:10.1029/2002JC001461, 2003.

Pedlosky, J., *Geophysical Fluid Dynamics*, 2nd ed., 710 pp., Springler-Verlag, New York, 1987.

Ralph, E. A., and P. P. Niiler, Wind driven currents in the tropical Pacific, *J. Phys. Oceanog.*, *29*, 2121–2129, 1999.

Reid, J. L., On the total geostrophic circulation of the North Atlantic ocean: Flow patterns, tracers, and transports, *Progr. Oceanogr.*, *33*(1), 1–92, 1994.

Reid, J. L., On the total geostrophic circulation of the Pacific ocean: Flow patterns, tracers, and transports, *Progr. Oceanogr.*, *39*(4), 263–352, 1997.

Reid, J. L., On the total geostrophic circulation of the Indian ocean: Flow patterns, tracers, and transports, *Progr. Oceanogr.*, *56*(1), 137–186, 2003.

Salmon, R. L., Lectures on Geophysical Fluid Dynamics, 400 pp., Oxford University Press, 1998.

Tapley, B. D., The gravity recovery and climate experiment (GRACE), *Supp. Eos Transactions of the AGU*, *78*(46), 163, 1997.

Uchida, H., and S. Imawaki, Eulerian mean velocity field derived by combining drifter and satellite altimeter data, *Geophys. Res. Lett.*, *30*(5), 1229, doi:10.1029/2002GL016445, 2003.

P. P. Niiler, Scripps Institution of Oceanography, University of California and San Diego, USA. (pniiler@ucsd.edu)

N. A. Maximenko, International Pacific Research Center, SOEST, University of Hawaii, USA. (nikolai@soest.hawaii.edu)

J. C. McWilliams, University of California, Los Angeles, USA. (jcm@ucar.edu)